Pulsar γ Rays from Polar Cap regions

James Chiang and Roger W. Romani

Dept. of Physics, Stanford University
Stanford, CA 94305-4060

Abstract

We investigate the production of pulsar gamma rays by energetic electrons flowing in the open-field region above pulsar polar caps. We have followed the propagation of curvature radiation from primary electrons, as well as hard synchrotron radiation generated by secondary pairs, through the pulsar magnetosphere for vacuum dipole open-field geometries. Using data from radio and optical observations we construct models for the specific geometries and viewing angles appropriate to particular pulsars. These detailed models produce normalized spectra above 10MeV, pulse profiles, beaming fractions and phase resolved spectra appropriate for direct comparison with COS-B and GRO data. Models are given for the Crab, Vela and other potentially detectable pulsars; general agreement with existing data is good, although perturbations to the simplified models are needed for close matches. We have also extended the calculations to the millisecond pulsar range, which allow us to produce predictions for the flux and spectra of populations of recycled pulsars and point to search strategies.

Introduction

Early observations of galactic γ-ray sources, culminating with the COS-B mission, showed that radio pulsars with high spin-down luminosities are the brightest sources in the sky and have provided substantial information on their pulse profiles and integrated spectra. Attempts to model the production of this radiation have concentrated on two scenarios: polar cap models with radiation generated by primaries accelerated over a pulsar polar cap surface (*e.g.* Daugherty and Harding, 1982) and "outer gap" models with acceleration occurring high in the open field zone (*e.g.* Cheng, Ho and Ruderman, 1986). Both of these pictures have had some success in reproducing global properties of the observed emission.

Recent developments suggest that improved versions of such calculations are now appropriate. Progress in polarization observations and modeling of radio pulsars (Lyne and Manchester, 1988; Rankin, 1990) have allowed the particular viewing geometries of individual objects to be determined in many cases. Further, with the advent of the GRO facility, it is likely that improved sensitivity on the brightest gamma ray pulsars will allow the observations of detailed pulse profiles and phase resolved spectra as well as the detection of several fainter objects. We are computing models for

these pulsars in both the 'Cap' and 'Gap' pictures which provide detailed spectral and pulse profile information that may be directly compared with these data. It appears that the phase resolved spectra, in particular, can provide a means of discriminating between these two classes of models. Further comparison of the models with the data should allow us to study perturbations to the basic magnetic field geometry and provide insights into the primary acceleration mechanisms.

A second arena in which improved calculations are now needed stems from the discovery of large numbers of recycled pulsars. These short period, low magnetic field objects have very long lifetimes and substantial spindown luminosities and thus have been proposed as possible gamma ray sources by several authors. However, no specific models for the luminosity and spectral behavior of recycled pulsars have been produced. We have computed such models for polar cap geometries. An important ingredient of these computations is a substantial coverage of the parameter space in pulsar period, magnetic field, and inclination which both highlight the differences in these scalings from those of the Crab-like pulsars and allows us to compute fluxes integrated over recycled pulsar populations.

Model Computations

In the present model, we confine origin of the outflowing relativistic primaries to the pulsar polar cap, as defined by the open field line region in the vacuum magnetic dipole model. When the inclination of the magnetic axis to the pulsar rotation axis $\alpha \neq 0$, then the locus of field lines defining the cap boundary will not, in general, be a circle. In addition, the line of sight swept out by the observer often lies at a substantial angle β with respect to the magnetic pole (*cf.* Figure 1).

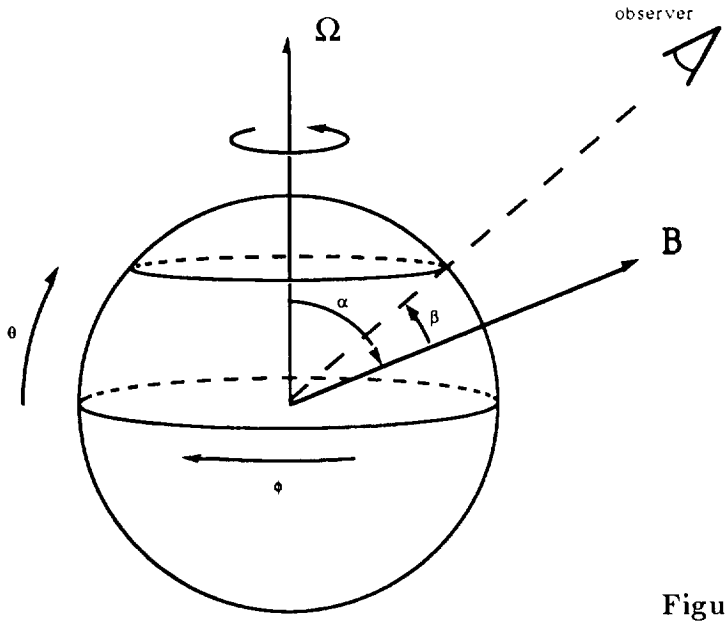

Figure 1. Magnetic Dipole Geometry

The model assumes that primary $e^{\pm}$ are accelerated in a small zone above the polar cap surface. In our simulation, $e^{\pm}$ are injected with $\Gamma \equiv E/m_e c^2$, distributed with the dipole field strength across the polar cap zone. Typically $\Gamma \sim 3 \times 10^7$ for these models, appropriate to the Ruderman and Sutherland (1975) model of the pulsar polar cap – different energies and allowance for an extended spectrum of primaries were shown to have a modest effect on the emergent γ radiation. In the spirit of Sturrock's (1971) pair cascade model and following the early computations of Harding (1981) and Daugherty and Harding (1982), we follow the curvature photons from these energetic primaries as they propagate through the rotating magnetosphere. Attenuation from magnetic pair production (Daugherty and Lerche, 1975) reduces the curvature spectrum, and for the chosen rays a Monte Carlo draw of the conversion points gives relativistic secondary pairs that synchrotron radiate in the strong magnetic field. Our computation evaluates this spectrum according to the distribution function of Erber (1966) in the frame co-moving with the e^+/e^-, discretizes and follows trajectories for the resultant photons as they propagate out of the pulsar magnetosphere.

Synchrotron photons of sufficient energy will further pair produce, and the propagation and attenuation of the resulting shower is followed to give γ spectra extending down to $\sim$ 10MeV in the observer's frame. Quantization of the synchrotron spectrum for very low pair energies has not been considered in detail, and may have some effect on the lowest energy bins in the final spectrum. By creating a new and substantially streamlined Monte Carlo code, we have been able to follow large numbers of primaries above the polar cap, allowing a calculation of the true spectra and pulse profile observed along a particular line of sight and comparison with the appearance of the pulsar from other directions for the model dipole geometry.

To compute the effective phases of the various photons (or, equivalently, the relative arrival times in the solar system barycenter) aberration of the photons from the rotating emission region has been treated. In addition, we consider the relative time delays in travel across the magnetosphere, which can amount to an appreciable fraction of the pulsar period, especially for curvature photons.

Individual Pulsar Models

Optical polarization data on the Crab (Kristian *et al.*, 1970) allow the geometry angles to be determined as $\alpha = 86°$, main pulse $\beta = -9.6°$, interpulse $\beta = 18°$. Similarly, radio data on Vela gives $\alpha = 90°$, $\beta = 6.4°$, where the statistical errors are small but certain systematic variations probably remain.

Since the dipole model for the pulse polarization sweep is generally successful, the radio emission should result from emission aberrated from the magnetic dipole axis. In figures 2-4 we indicate the phase of the center of the radio main pulse as a function of the height of the radio pulse production in the open field line zone (in units of r_{LC}, right scale). This phase is that at infinite radio frequency. Radio emission heights of several tenths of the light cylinder distance are suggested by some other observations and can explain the offset between the gamma emission and the radio pulse seen for the Crab.

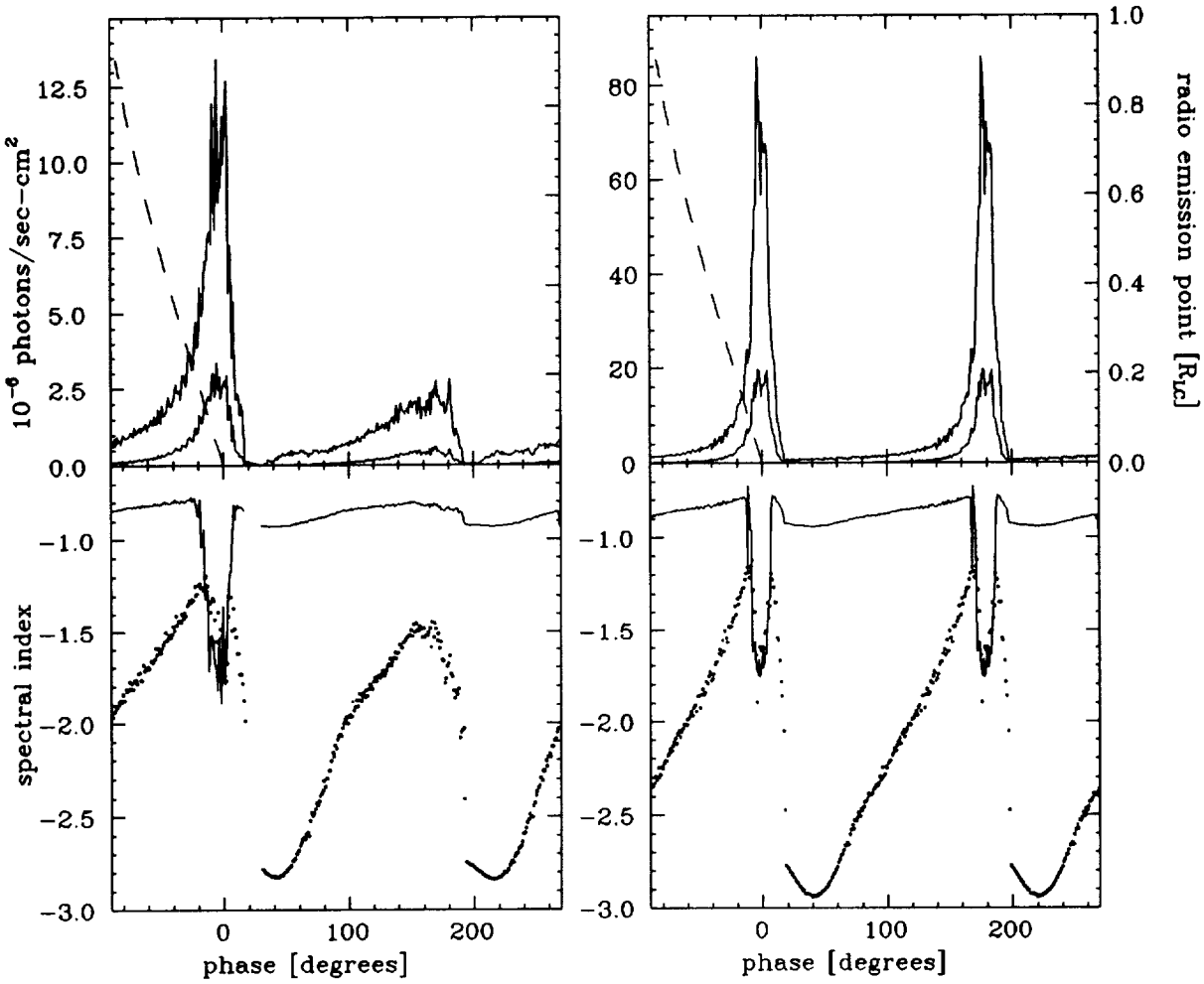

Figures 2,3. Light curves and spectral index variations for Crab(left) and Vela (right).

In figures 2 and 3, we show the results of polar cap calculations for Crab and Vela, respectively. In the upper panel pulse profiles are shown for energies above 100MeV and for energies above 500MeV. Fluxes are total count rates with the normalization determined by a corotation charge density of primaries flowing at the polar cap and by the pulsar distance. Note that the Crab interpulse does not cross the synchrotron core and so does not have a cusp due to the low energy emission; clearly perturbations to the simple dipole geometry are needed in this case. In the lower panels, we show the phase resolved spectral indices as determined from simple power law fits to the ranges 10MeV-100MeV (upper curve) and 100MeV-1GeV (lower points). Clearly a power law is a poor fit to the higher energy range, as the cut off of the curvature spectrum moves well below 1GeV off the center of the pulse, causing large variations in the fitted value. In the bright center of the pulse the spectral index approaches -2, but is typically much larger (harder spectrum) between the pulses and in the crab second pulse. Note that the inevitable admixture of residual background at these low count rates will bias all the spectral index values closer to -2.

In figure 4, we show the light curves predicted for three nearby pulsars which have been

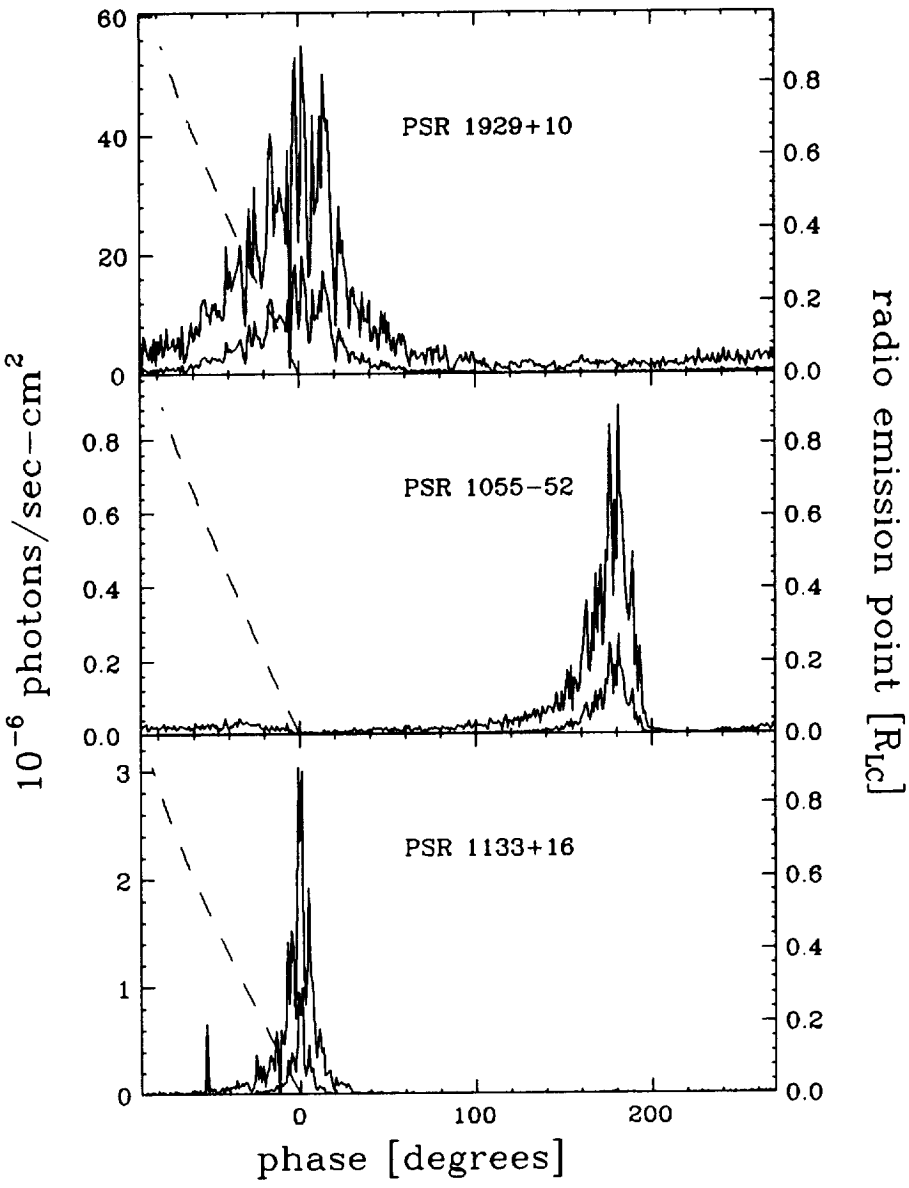

Figure 4. Some potentially bright pulsars.

suggested as candidates for detection by the EGRET experiment on GRO (Buccheri and Schoenfelder, 1989). The energy ranges and flux normalizations are as for Crab and Vela. PSR1055-52 is a nearly orthogonal rotator dominated by an interpulse, PSR1133+16 has $\alpha = 51.3°$, and PSR1929+10 is a nearly aligned rotator with a broad pulse. Emission geometries are determined from radio polarization and pulse-width data (Lyne and Manchester, 1988).

Integration along our model slice gives the expected time-average spectrum of the pulsar. In figure 5, we compare the results for Crab and Vela with the spectrum averaged over all viewing angles. There are significant differences for both models. In particular, a low-energy deficit for the

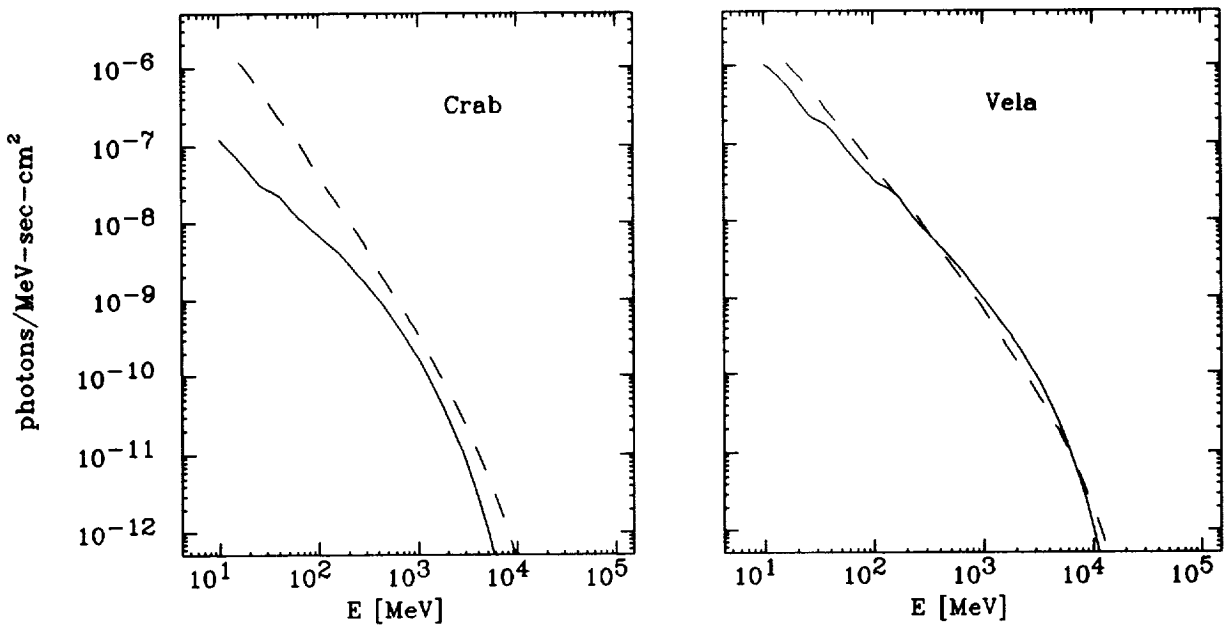

Figure 5. Phase (solid) and all-viewing-angle (dashed) averaged spectra for Crab and Vela.

Crab slice indicates that there should be perturbations from the simple dipole model that place the second pulse line of sight closer to the magnetic axis.

Scaling Laws for Recycled Pulsars

We have computed families of models to find the average emission of recycled pulsars and to compare the scalings of the integrated flux and the spectral indices with pulsar parameters with those found for high field (Crab-like) models. Typical recycled pulsar models have $B = 10^8 - 10^{10}$G and $P = 1 - 33$ms. The models show that except for the highest field recycled pulsars, synchrotron emission is unimportant. Also, with the very large open field line region of fast pulsars, most lines of sight see comparable integrated fluxes. The scaling with P of the luminosity and the spectral indices in two energy ranges is shown in figure 6.

With large opening angles, small radii of curvature and the dominance of curvature spectra we find that the total ($\geq$10MeV) luminosity scales as

$$F \sim 3.5 \times 10^{33} P_s^{-1.4} B_{12}^{0.95} \mathrm{erg/s}.$$

This is to be compared with the Crab-like objects for which

$$F \sim 6.4 \times 10^{32} P_s^{-2.2} B_{12}^{1.1} \mathrm{erg/s}.$$

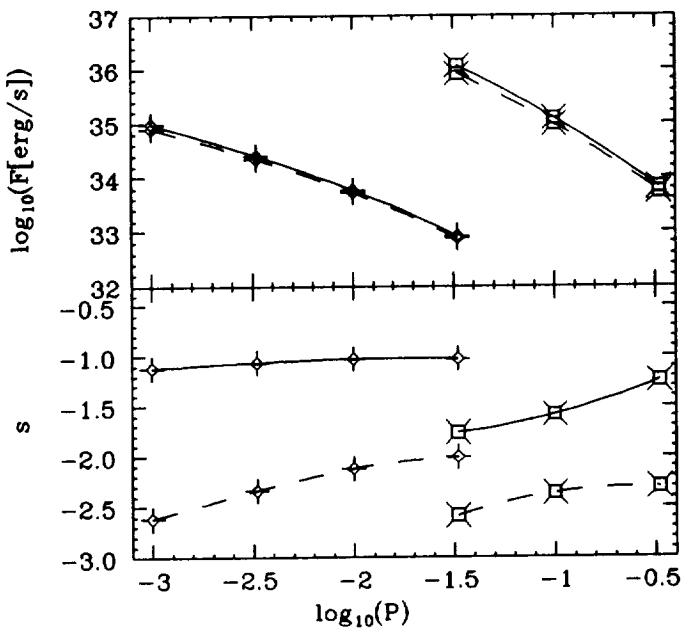

Figure 6. Period Dependence of Pulsar Fluxes and Spectral Indices

For low magnetic fields the spectral slopes in the low energy range (10MeV-1GeV) are relatively flat and do not strongly depend on P or B. This is as expected since pair attenuation of the curvature spectrum and the resultant synchrotron radiation is weak. For higher energies (1GeV-10GeV) the fitted spectral slope is sensitive to the curvature cut-off in the varying cap size, giving spectral indices $s \approx -1.59 - 0.08\log(B_{12}) + 0.4\log(P_s)$. Thus millisecond pulsars have substantially harder spectra than their high field cousins. At high energies the spectral cut-off depends fairly strongly on P.

Conclusions and Work in Progress

When normalized to a vacuum co-rotation charge density flowing through the cap surface, polar cap models reproduce the overall flux and spectrum of observed gamma ray pulsars at energies $\geq$10MeV quite well. These cap models produce beams of secondary synchrotron photons tightly collimated to the dipole axis. It is clear that models with lines-of-sight at large impact parameters to the field axis will not reproduce the cusp-like profiles of Crab and Vela. For the angles determined from low frequency observations the match of the models to observed profiles is reasonable at high (EGRET) energies, but does not fit in detail. The best hope for discrimination of these models arises from the phase resolved spectra: lowered fields off the pulse center cause harder curvature spectra, while simultaneously lowering the high energy cut-off.

For recycled pulsars the predicted fluxes and fairly hard spectral indices below 1GeV bode well for possible detections. The combined fluxes from groups of such objects, especially the known large populations of recycled pulsars in globular clusters, will also make interesting targets. We are presently integrating over populations of cluster pulsars to find the energy range most suitable for searches for such objects. As a test case, we are deriving upper limits from the COS-B data base and are using these data as a guide to appropriate search strategies.

The computations with specific geometries should be viewed as an interpretive tool for the refinement of acceleration and emission models. In this spirit, we are extending the calculation to a realization of the 'outer gap' picture, as described by Cheng, Ho and Ruderman. Inclusion of geometric effects will produce significant signatures in the pulse phase fluxes and spectra. Impending observations are likely to allow good discrimination among different models. An important feature of these computations is the production of normalized fluxes and energy ranges appropriate to particular GRO instruments. This should allow ready adoption and use by scientists working directly with the data.

References

Buccheri, R. and Schoenfelder, V. 1989, in *Timing Neutron Stars*, Oegelman and van den Huevel, eds. (Kluwer:Dordrecht), 419.

Cheng, K.S., Ho, C. and Ruderman, M. 1986, *Ap.J.*, **300**, 522.

Daugherty, J.K. and Harding, A.K. 1982, *Ap.J.*, **252**, 337.

Daugherty, J.K. and Lerche, I. 1975, *Ap. Sp. Sci.*, **38**, 437.

Erber, T. 1966, *Rev. Mod. Phys.*, **38**, 626.

Harding, A.K. 1981, *Ap.J.*, 245, 267.

Kristian, J., Visvanathan, N, Westphal, J.A. and Snellen, G.H. 1970, *Ap.J.*, **162**, 475.

Lynn, A. and Manchester, R.M. 1988, *MNRAS*, **234**, 477.

Rankin, J.M. 1990, *Ap.J.*, **352**, 247.

Ruderman, M.A. and Sutherland, P.G. 1975, *Ap.J.*, **196**, 51.

Sturrock, P.A. 1971,*Ap.J.*, **164**, 529.